First-principles simulation of the interaction between adamantane and an atomic-force-microscope tip

G. P. Zhang
Department of Physics, Indiana State University, Terre Haute, Indiana 47809, USA

Thomas F. George
Office of the Chancellor and Center for Molecular Electronics, Department of Chemistry & Biochemistry and Department of Physics & Astronomy, University of Missouri–St. Louis, St. Louis, Missouri 63121, USA

Lahsen Assoufid
X-ray Science Division, Argonne National Laboratory, 9700 South Cass Avenue, Argonne, Illinois 60439, USA

G. Ali Mansoori
Department of Bioengineering and Department of Chemical Engineering, University of Illinois at Chicago, Chicago, Illinois 60607-7052, USA

(Received 25 July 2006; revised manuscript received 3 October 2006; published 12 January 2007)

A first-principles calculation is performed to investigate the interaction between adamantane and an atomic-force-microscope tip. By holding the tip at different distances from adamantane, three scans across two surfaces, one with a carbon atom at the center and the four other equivalent atoms at the corners, and the other with three equivalent carbon atoms in the front and three other atoms in the back forming a hexagon shape, reveal the detailed morphology of adamantane. For the first scan surface, a huge potential energy change is observed when the tip is close to adamantane, which results from the strong interaction from two hydrogen atoms attached to the center carbon atom. On the second scan surface, a radial scan shows the maximum force constant of 2 hartrees/Å^2. This is proof of the hardness of adamantane. The rotational scan along the second surface reveals a systematic change in the potential energy as the tip is moved away from adamantane. Due to the existence of two types of carbon atoms in adamantane, the original potential maxima are shifted 60° to new maxima. Between these maxima, there is a flat region. Finally, an *x-y* force scan over the above two surfaces is performed, where two distinctive images of hydrogen atoms are found. These results are detectable experimentally.

DOI: 10.1103/PhysRevB.75.035413 PACS number(s): 68.35.−p, 62.25.+g, 68.37.Ps, 61.66.Hq

I. INTRODUCTION

Adamantane (from $\alpha\delta\alpha\mu\alpha\chi$, the Greek word for diamond) was first isolated from petroleum in former Czechoslovakia by Landa, Machacek, and Mzourek in 1933.[1] Successful isolation and characterization of higher diamondoids has revitalized the interest in these compounds.[2] Diamondoids represent a group of hydrocarbon molecules with a structure similar to part of a typical diamond structure.[3] In fact, one can successively construct different diamondoids by excising from the diamond crystal lattice and saturating dangling carbon bonds with hydrogen atoms. Adamantane is the smallest such compound and has important pharmaceutical applications such as adamantane antiflu drugs. Molecular simulation studies[4] reveal more details about these compounds and suggest some possible applications in nanotechnology. Diamondoids have been used to test quantum confinement limits.[5] Recently, an adamantane moiety was directly attached to a blue-light-emitting polymer.[6] Its mechanical properties in particular have attracted attention, and a high-pressure study has been done on adamantane.[7] Li *et al.*[8] synthesized four tripod 1,3,5,7-tetrasubstituted adamantanes for atomic-force-microscopy applications. It has been shown that adamantane molecules can be used as atomic-force-microscope tips.[9]

Motivated by these previous studies, we perform a first-principles calculation of the adamantane mechanical properties. We simulate an atomic-force-microscope (AFM) study on the top of adamantane, where we model the AFM tip with one gold atom. Three representative scans are done: a rotational scan over the surface with a carbon atom at the center and four other equivalent atoms at the corners; a radial scan; and a rotational scan along the surface with three equivalent carbon atoms in the front and three other atoms in the back forming a hexagon shape. Our simulation shows that the AFM tip can directly map out the adamantane morphology very accurately. In particular, a π period of potential energy change in the face-centered scan is found. We also see a sharp potential change when the tip is close to the surface. In order to measure the force constant, we perform a radial scan along the second surface. The maximum force constant, which is at 1 Å from adamantane, is 2 hartrees/Å^2. This demonstrates the hardness of the material. If we rotate and scan the adamantane surface, depending on the distance from the adamantane, there is a transition from a three-peak structure to a six-peak structure and finally back to the three-peak structure. This transition directly reflects the local morphology of adamantane. We expect these results are demonstrable experimentally.

The paper is arranged as follows. In Sec. II, we present our theoretical formalism and structural optimization. Sec-

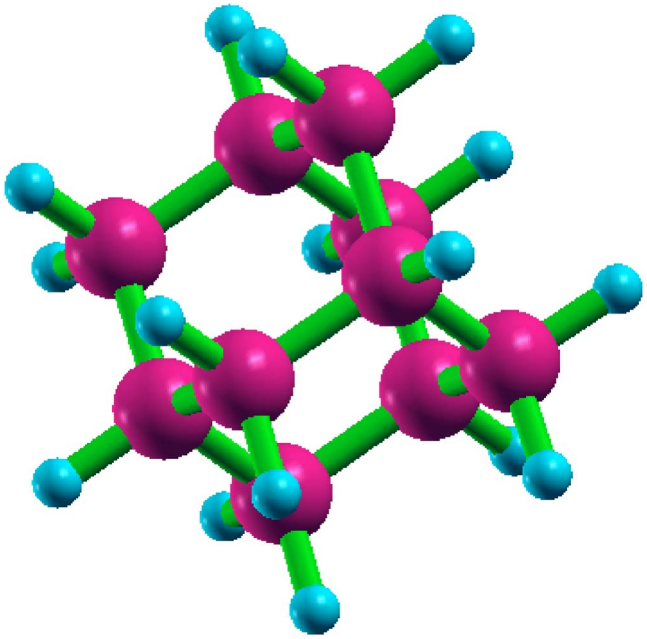

FIG. 1. (Color online) Adamantane structure. The coordinates are listed in Table I.

tion III shows the simulation of the interaction of an AFM tip and adamantane, followed by a two-dimensional image of forces in Sec. IV. Finally, we conclude our paper in Sec. V.

II. THEORETICAL FORMALISM AND STRUCTURAL OPTIMIZATION

Adamantane's chemical formula is $C_{10}H_{16}$. Its group symmetry is T_d, where the structure formed by carbon atoms is similar to the diamond structure (see Fig. 1). In the following, we will use the diamond lattice to help us identify the carbon atoms in adamantane. Similar to diamond, there are also two types of carbons: one on the face center and the other at the tetrahedral center. However, different from diamond, in adamantane each of the six carbon atoms at the six face centers of a cube is saturated by two hydrogen atoms, while each of the other four carbons at the four tetrahedral centers is saturated with one hydrogen atom. These tetrahedral-centered carbon atoms and their respective hydrogen atoms are along four diagonal directions of the cube. If we rotate adamantane along the [100] direction so that one face-centered atom is at the center and the other four are at the corners, we end up with a squarelike structure (see the top structure in Fig. 2). The scan in this orientation will be called the [100] scan. On the other hand, if we project along one of the diagonal directions, i.e., [111], with one tetrahedral-centered carbon atom and hydrogen atom in the back center, three face-centered carbon atoms and three tetrahedral-centered carbon atoms effectively form a hexagon shape with these two types of atoms alternating. We call this the [111] scan.

Our simulation starts with the structural optimization of adamantane. We use the NIST structure as our starting structure.[10] The calculation[11] is done using three different

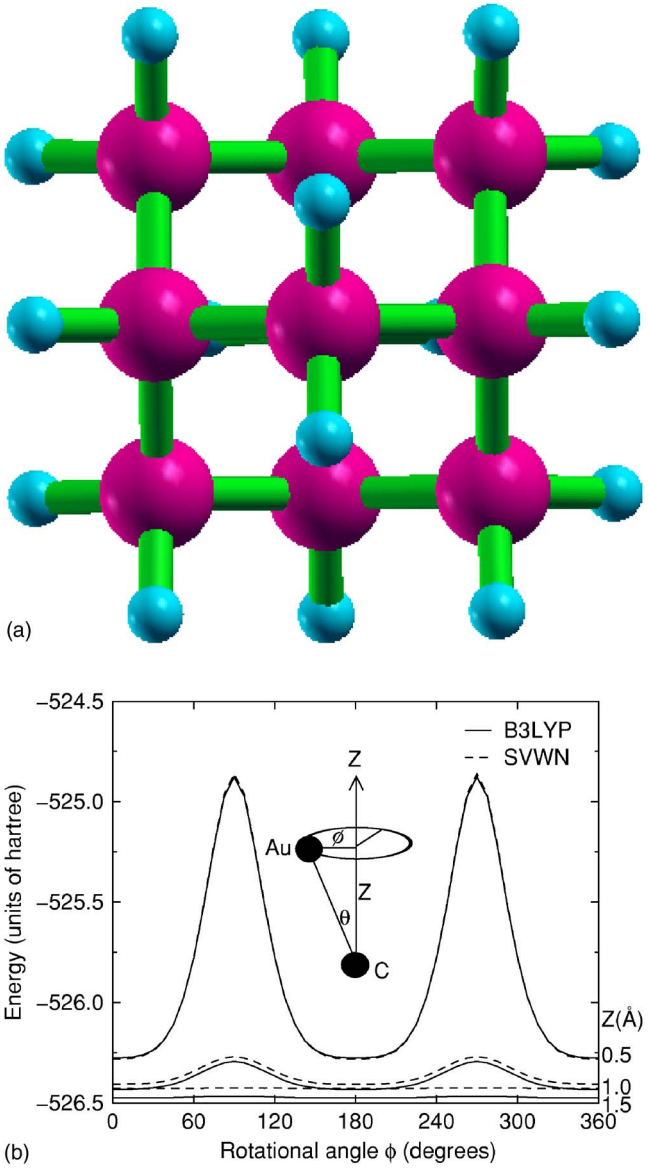

FIG. 2. (Color online) Top: Adamantane oriented along the [100] direction. The z axis points in the [100] direction and through the center carbon atom. Bottom: Energy change as a function of the rotational angle ϕ at z=0.5, 1.0, and 1.5 Å. The solid line is from the B3LYP calculation. The dashed lines, vertically shifted, refer to the SVWN results. Inset: Scanning geometry of the gold atom. The origin is at the center carbon atom. θ is the polar angle and ϕ is the azimuthal angle.

methods:[12] Slater exchange and Vosko, Wilk, and Nussair correlation functional or SVWN(5),[13] second-order Moller-Plesset and full-inner core electron perturbation method (or MP2FU) and Becke's 91 parameters and Becke, Lee, Yang and Parr functional (B3LYP).[14] The basis set for both the carbon and hydrogen atoms is a correlation-consistent polarized valence double-ζ basis (cc-pvdz). For carbon, there are 3s, 2p, and 1d functions, and for hydrogen, it includes 2s and 1p functions. We do not impose any constraints on the optimization, which gives us a well-converged structure. The optimized structure is shown in Fig. 1. The explicit coordinates are listed in Table I, from which we find that the

TABLE I. Optimized adamantane coordinates. The coordinate system is different from those in Figs. 2 and 3.

Atom	x (Å)	y (Å)	z (Å)
C1	0.892038	0.892038	0.892038
C2	−0.892038	−0.892038	0.892038
C3	−0.892038	0.892038	−0.892038
C4	0.892038	−0.892038	−0.892038
C5	0.000000	0.000000	1.780097
C6	0.000000	0.000000	−1.780097
C7	0.000000	1.780097	0.000000
C8	0.000000	−1.780097	0.000000
C9	1.780097	0.000000	0.000000
C10	−1.780097	0.000000	0.000000
H1	1.529129	1.529129	1.529129
H2	−1.529129	−1.529129	1.529129
H3	−1.529129	1.529129	−1.529129
H4	1.529129	−1.529129	−1.529129
H5	2.438759	−0.626778	0.626778
H6	2.438759	0.626778	−0.626778
H7	−2.438759	−0.626778	−0.626778
H8	−2.438759	0.626778	0.626778
H9	−0.626778	2.438759	0.626778
H10	0.626778	2.438759	−0.626778
H11	0.626778	−2.438759	0.626778
H12	−0.626778	−2.438759	−0.626778
H13	−0.626778	0.626778	2.438759
H14	0.626778	−0.626778	2.438759
H15	0.626778	0.626778	−2.438759
H16	−0.626778	−0.626778	−2.438759

nearest-neighbor distance is 1.543 Å and C-H bond length is 1.104 Å. This can be compared with the experimental results for the average C-C bond length as 1.54 Å and C-H as 1.12 Å.[15] Our total energy of adamantane is −390.740 a.u., which is slightly lower than a previous self-consistent-field result of −388.097 a.u. using a Dunning double-ζ basis.[16] Given that different bases and methods are used in these studies, this agreement is good.

We show eigenvalues for all the occupied states and 30 unoccupied states in Table II. The first two rows in the table are assigned to the carbon 1s core electron. This core energy is slightly lower than the free carbon 1s energy of about −10.3 a.u., which can be tested experimentally. The electronic states at −0.76 a.u. mainly consist of carbon 2s electrons, but hybridization is obvious among these states. For other states, the hybridization between the s and p orbitals becomes much stronger. For instance, three degenerate states at −0.277 19 a.u., just below the Fermi level, are a result of sp^2-sp^3 hybridization.

Both of our optimized structure and electronic states are fully consistent with the previous study.[10] The energy gap of 0.317 24 hartrees also agrees with another study,[17] but it is larger than the gap of 7.622 eV obtained by McIntosh *et al.*[18] who use Troullier-Martins pseudopotentials. Such a difference is expected since the results certainly depend on the basis function, density functional, and techniques used. To validate our claims, we investigate how large the energy gap change can be among different methods. We find that for the same basis the energy gap can range from 0.562 48 a.u. (MP2), 0.317 24 a.u. (B3LYP), 0.268 11 a.u. (SVWN), 0.2546 a.u. [Perdew-Burke-Ernzerhot] (PBE)[19] to 0.24633 a.u. (SVWN5). This difference is important for electronic and optical properties, but does not affect the mechanical property studies here as seen below.

III. SIMULATION OF THE INTERACTION OF AN AFM TIP AND ADAMANTANE

Once we find the optimized adamantane structure, we fix it for further AFM studies.[20] Currently, we limit ourselves to the static AFM simulation.[21] In order to simulate the gold atom, we use the pseudopotential from Figgen *et al.*[22] The basis set is the pseudopotential-based correlation-consistent polarized valence double-ζ basis.[23] We have tested both the pseudopotential and basis set by comparing the results for a gold atom with previous calculations.[24] We also have tested the GAUSSIAN 03 results against the MOLPRO calculation.[25] In both cases a consistency is found. In real experiments, normally it is very difficult to know beforehand the orientation of adamantane. In this paper, as a first attempt, we choose two representative orientations and three scans by either radially moving away from the sample or rotating the sample. We start with the [100] scan. In the inset of Fig. 2, we schematically show the scan direction. The origin of the z axis is at the center carbon atom. The gold atom makes an angle of $\theta=80^\circ$ with respect to the z axis. Choosing too large an angle will diminish the signal change from the sample since the tip is then too far away from the sample. We situate the AFM tip with $z=0.5$, 1.0, and 1.5 Å above the center atom (see the inset in Fig. 2). In real experiments, the tip is about 4–5 Å from the sample, but we find the overall energy change is similar to the $z=1.5$ Å case though as expected the overall energy change at larger distances is much smaller. The rotational axis or z axis is perpendicular through the center atom and out of the page. Note for convenience that we choose different z axes for different scans.

The results are shown in Fig. 2. We first look at $z=0.5$ Å. There is a huge potential energy change as we scan from $\phi=0^\circ$ to 360°. Two maxima are at $\phi=90^\circ$ and 270°. The maximum change is 1.4 hartrees. Note that this big change is a direct result of the close proximity of the gold atom to adamantane. We find these two peaks to result from the strong repulsion between the tip and two hydrogen atoms. To verify it, we use different methods and find a similar result. For instance, the SVWN potential gives an identical result (see the dashed line in Fig. 2), where we vertically shift the SVWN results for an easy comparison. This is the first proof that validates our calculation and verifies the well-known fact that the mechanical properties are much less sensitive to the methods used. The width ΔD of these peaks measures the electron cloud spreading in the vicinity of the hydrogen atom and can be computed from $\Delta D=(z\tan\theta)\Delta\phi=0.8$ Å. When we move the tip away from adamantane, the potential change

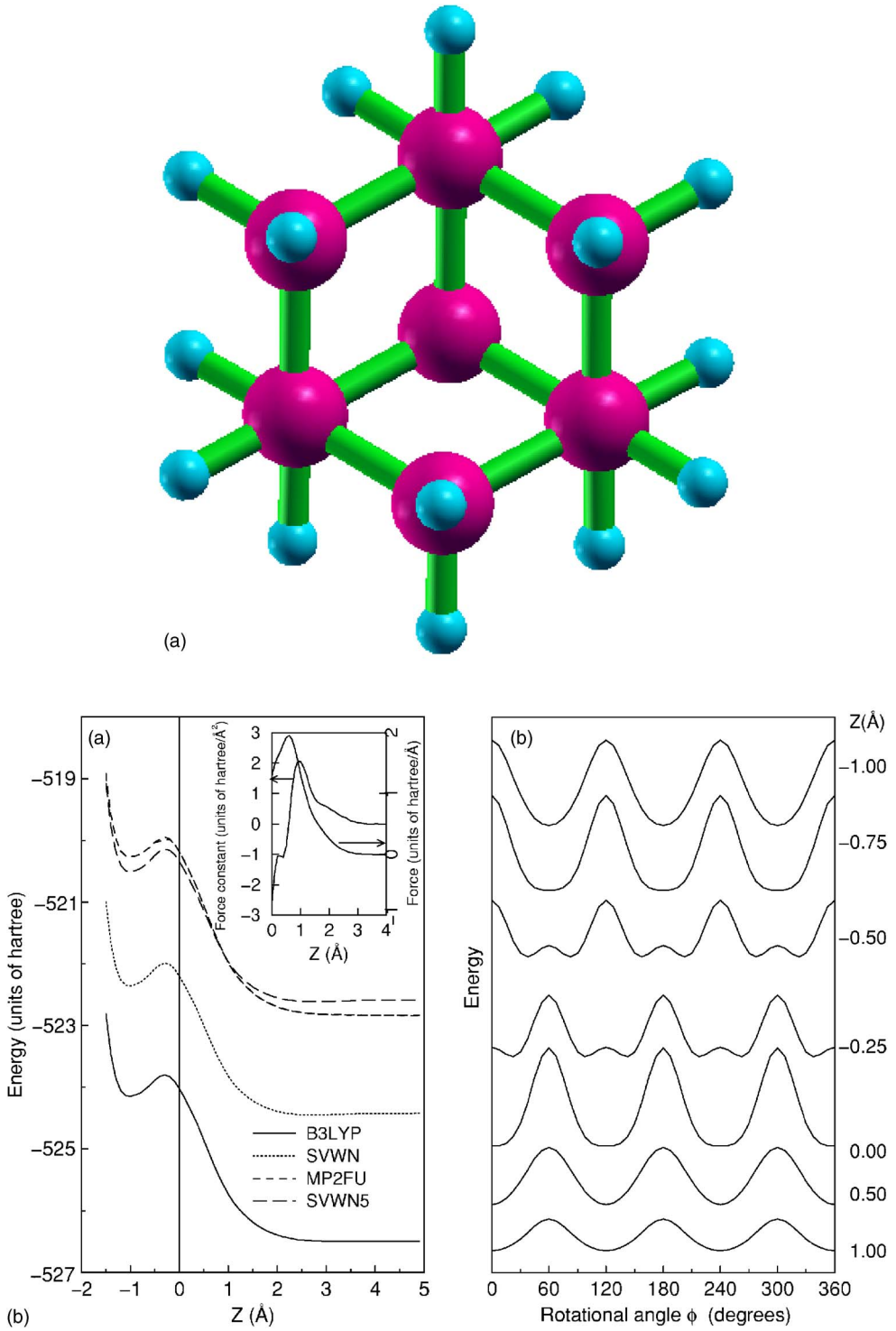

FIG. 3. (Color online) Top: Adamantane oriented along the [111] direction. The z axis is also along this direction. Bottom: (a) Total energy change as a function of the distance z between the tip and adamantane. The gold atom scans radially away from adamantane. Four different methods reveal a similar potential energy change. Inset: Force constant and force versus z. (b) Potential energy change obtained at the B3LYP level as a function of ϕ at several distances z, similar to Fig. 2. A clear peak change is noticed as the tip moves away from adamantane.

drops substantially. At $z=1.5$ Å, the change is tiny.

For the [111] scan, we orient adamantane as shown in Fig. 3 with the (111) plane in the front and the center carbon atom in the back, which is created by projecting along the [111] direction. We set our z axis through the center atom and perpendicular out of the page. The origin of the axis is at the center of the triangle formed by three face-centered carbon atoms (see the three carbon atoms with two hydrogen atoms attached). Two different scans have been performed. One is the radial scan, where the tip moves along the z axis away

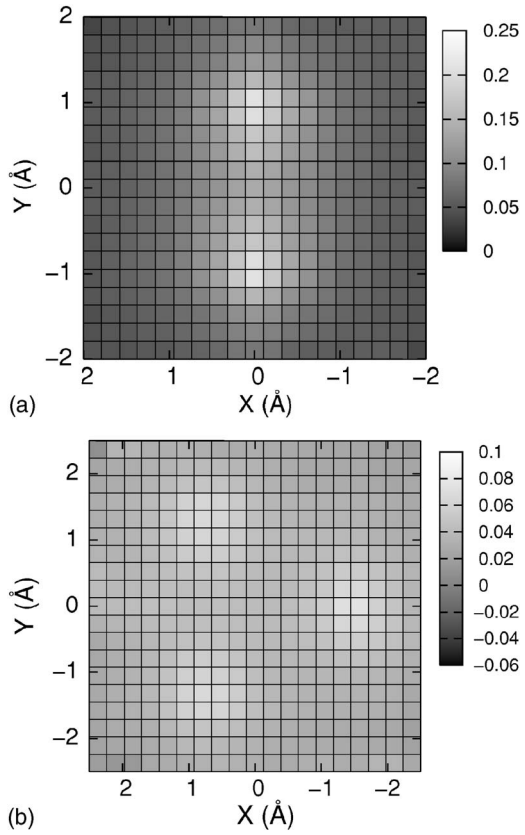

FIG. 4. *x-y* scan image for (a) (100) and (b) (111) surface. The bright spots represent where the hydrogen atoms are located, and the gray scale on the right shows the magnitude of the force. For (a), the tip is 1.2 Å away from the center carbon atom; for (b), the tip is 1.8 Å away from the center of the triangle formed by the three outermost carbon atoms.

from adamantane. The results are shown in Fig. 3(a), where the thin vertical line refers to the origin or the above triangle center. We first focus on the B3LYP results. As one moves the tip close to adamantane, the potential increase sharply, with a local maximum appearing slightly below $z=0$. After that, a local minimum appears at about 1 Å. We should note that the diameter of the hole is only 2.955 Å, while the gold atom radius is 1.79 Å. Normally, the gold atom cannot enter the cavity. Our purpose here is to explore some possible scenarios that may occur in a real experiment. For instance, one may also consider using a carbon atom or its cluster as a tip, whose radius is much smaller. By taking the second derivative with respect to z, we compute the force constant. As can be seen from the inset, the force constant reaches a maximum of 2 hartrees/Å at $z=1$ Å. This value is about 1.5 times the force constant for bond stretching in C_{60}, which demonstrates the tremendous hardness of adamantane. Also shown in the inset is the force as a function of the distance between the gold atom and adamantane. In order to check whether the B3LYP results are reliable, we have performed a similar calculation at the SVWN, MP2FU, and SVWN5 levels, whose results are shown by the dotted, short-dashed, and long-dashed lines, respectively. Except for the vertical shifts, both the perturbative and density-functional results all agree with the same trend of the energy change as the B3LYP calculation demonstrates. This is another proof of the reliability of our calculation.

Next, we perform a rotational scan along the z axis. Although we only show the B3LYP results in Fig. 3(b), we emphasize that results by other methods are similar. The scan geometry is similar to the face-centered scan. The position of the tip is situated at several different distances from adamantane. The scan starts from $z=-1.0$ Å. Different from the [100] scan, there are three peaks 120° apart. We find these

TABLE II. Electronic states at the optimized geometry. All the units are in hartrees. 39 states are occupied, with the first ten being core states. Column 1 indicates either the occupied or unoccupied states. Columns from 2 to 6 refer to the eigenvalues of these states.

Occupied	−10.18081	−10.18081	−10.18081	−10.18077	−10.17446
Occupied	−10.17446	−10.17442	−10.17442	−10.17442	−10.17438
Occupied	−0.86514	−0.76307	−0.76307	−0.76307	−0.66075
Occupied	−0.66075	−0.57673	−0.57673	−0.57673	−0.51662
Occupied	−0.45284	−0.44438	−0.44438	−0.44438	−0.40047
Occupied	−0.40047	−0.40047	−0.38601	−0.38601	−0.38601
Occupied	−0.32514	−0.32514	−0.32073	−0.32073	−0.32073
Occupied	−0.27719	−0.27719	−0.27719		
Unoccupied	0.04005	0.08845	0.08845	0.08845	0.10152
Unoccupied	0.10152	0.10152	0.12534	0.12724	0.12724
Unoccupied	0.15916	0.15916	0.15916	0.17516	0.17516
Unoccupied	0.17516	0.21343	0.21343	0.21343	0.21792
Unoccupied	0.21792	0.24554	0.26133	0.26133	0.26133
Unoccupied	0.28735	0.28735	0.28735	0.42580	0.42580
Unoccupied	0.42580	0.44108	0.45486	0.45486	0.45486
Unoccupied	0.51581	0.51581	0.56775	0.56775	0.56775
Unoccupied	0.58737	0.58737	0.61447	0.61447	0.61447
Unoccupied	0.62301	0.62301	0.62301	0.62716	0.65956

peaks to result from three tetrahedral-centered carbon atoms. In the top structure in Fig. 3, these carbon atoms appear to have "three" hydrogen atoms, though in fact the other two hydrogen atoms belong to the face-centered atoms which happen to be right behind the tetrahedral-centered atoms. When we move the tip slightly out to $z=-0.75$ Å, we find that while the peak height stays roughly the same, the valleys become flat, which is the first indication of contribution from other types of carbon atoms at $\phi=60°$, 180°, and 300°. This is indeed true as smaller peaks start to grow at these angles when we move the tip to $z=-0.5$ Å. Interestingly, these original peaks at $\phi=120°$, 240°, and 360° are sharply reduced at $z=-0.25$ Å and almost disappear at $z=0$ Å. In the meantime, three new peaks become very large. Note again that there is a flat region on the curve around those peak positions at $\phi=60°$, 180°, and 300°. These flat regions are similar to what we have seen in the [100] scan in Fig. 2. They are likely to be probed by experiments.

In order to understand the reason behind the above changes in the peaks, we carefully match the changes with the adamantane structure. We find that at $z=-1.0$ Å, the tip experiences a stronger interaction with the tetrahedral-centered carbon atoms since they are geometrically closer to the tip, while a much weaker interaction is from the face-centered carbon atoms. This produces only three large peaks on the rotational scan. However, when we move to $z=-0.5$ Å, the tip is now also close to the face-centered carbon atoms, which leads to small humps on the curves. Since tetrahedral-centered and face-centered atoms are 60° apart, this explains why these small humps are shifted 60° from those large peaks. As we move away from adamantane, the relative magnitudes between these two groups of peaks are swapped since now the tip is closer to the face-centered atoms. At $z=0$ Å, although the contribution from the tetrahedral-centered atoms is weaker, the flat region between two peaks is a manifestation of their existence. This can be verified by moving the tip further away from adamantane, whereby the flat region becomes a valley now. We should mention that while in Fig. 3(b) the tip-sample distance is shown up to just 1 Å, the results at larger distances are similar, though the changes are smaller.

IV. TWO-DIMENSIONAL FORCE IMAGE OF ADAMANTANE

Finally, we also perform an *xy* force scan, where one scans over (100) and (111) surfaces. The scanning step is 0.5 Å along both the *x* and *y* directions. For the [100] scan, the *x* and *y* ranges are both from −2.0 to 2.0 Å, while for the [111] scan, the ranges are from −2.5 to 2.5 Å since the hexagon surface is wider. For the [100] scan, the tip is situated 1.2 Å above the center carbon atom. For the [111] scan, the tip is situated 1.8 Å above the center of the triangle. At each (x,y) point, we perform three calculations in order to compute the force. (we should point out that these calculations are very time consuming). Figure 4(a) shows the force along the *z* direction, where we use the intensity to show the magnitude of the force. One sees that there are two bright spots, which we know from the geometry of adamantane to correspond to the two outermost hydrogen atoms. Figure 3(b) shows a scan over the (111) surface. Different from the [100] scan, there are three bright spots in this picture, corresponding to the three hydrogen atoms. These distinctive features are expected to show up in real experiments.

V. CONCLUSION

In conclusion, we have performed a first-principles simulation to investigate how an AFM tip interacts with adamantane. It is found that the AFM tip is able to detect the sharp potential change in adamantane. For the scan along the [111] direction, we estimate the maximal force constant to be 2 hartrees/Å^2, which is an indication of the excellent mechanical properties of adamantane. We expect real experiments can probe these detailed changes. However, if the experimental tip contains more atoms, then the experimental results would be an average of the theoretical results.

ACKNOWLEDGMENTS

We would like to thank Eric Glendening for numerous helpful discussions on the details of the GAUSSIAN package. This work was supported by the U.S. Army Research Office under Contract No. W911NF-04-1-0383 and the U.S. Department of Energy under Grant No. DE-FG02-06ER46304. It was also supported by a Promising Scholars grant from Indiana State University.

[1] S. Landa, V. Machacek, and J. Mzourek, Chem. Listy **27**, 415 (1933); R. C. Fort, Jr., *Adamantane: The Chemistry of Diamond Molecules* (Marcel-Dekker, New York, 1976).

[2] J. E. Dahl, S. G. Liu, and R. M. K. Carlson, Science **299**, 96 (2003); A. P. Marchand, *ibid.* **299**, 52 (2003).

[3] G. A. Mansoori, *Principles of Nanotechnology* (World Scientific, Singapore, 2005).

[4] D. W. Brenner, O. A. Shenderova, D. A. Areshkin, J. D. Schall, and S.-J. V. Franklan, Comput. Model. Eng. Sci. **3**, 643 (2002); K. E. Drexler, *Nanosystems: Molecular Machinery, Manufacturing, and Computation* (Wiley, New York, 1992).

[5] T. M. Willey, C. Bostedt, T. van Buuren, J. E. Dahl, S. G. Liu, R. M. K. Carlson, L. J. Terminello, and T. Moller, Phys. Rev. Lett. **95**, 113401 (2005).

[6] S. Zheng, J. Shi, and R. Mateu, Chem. Mater. **12**, 1814 (2000).

[7] N. Arul Murugan, R. S. Rao, S. Yashonath, S. Ramasesha, and B. K. Godwal, J. Phys. Chem. B **109**, 17296 (2005).

[8] Q. Li, A. V. Rukavishnikov, P. A. Petukhov, T. O. Zaikova, C. Jin, and J. F. Keana, J. Org. Chem. **28**, 4862 (2003).

[9] S. Yasuda, I. Suzuki, K. I. Shinohara, and H. Shigekawa, Phys.

Rev. Lett. **96**, 228303 (2006).

[10] NIST Computational Chemistry Comparison and Benchmark Database, NIST Standard Reference Database Number 101 Release 12, August 2005, edited by Russell D. Johnson III, http://srdata.nist.gov/cccbdb

[11] M. J. Frisch, G. W. Trucks, H. B. Schlegel, G. E. Scuseria, M. A. Robb, J. R. Cheeseman, J. A. Montgomery, Jr., T. Vreven, K. N. Kudin, J. C. Burant, J. M. Millam, S. S. Iyengar, J. Tomasi, V. Barone, B. Mennucci, M. Cossi, G. Scalmani, N. Rega, G. A. Petersson, H. Nakatsuji, M. Hada, M. Ehara, K. Toyota, R. Fukuda, J. Hasegawa, M. Ishida, T. Nakajima, Y. Honda, O. Kitao, H. Nakai, M. Klene, X. Li, J. E. Knox, H. P. Hratchian, J. B. Cross, C. Adamo, J. Jaramillo, R. Gomperts, R. E. Stratmann, O. Yazyev, A. J. Austin, R. Cammi, C. Pomelli, J. W. Ochterski, P. Y. Ayala, K. Morokuma, G. A. Voth, P. Salvador, J. J. Dannenberg, V. G. Zakrzewski, S. Dapprich, A. D. Daniels, M. C. Strain, O. Farkas, D. K. Malick, A. D. Rabuck, K. Raghavachari, J. B. Foresman, J. V. Ortiz, Q. Cui, A. G. Baboul, S. Clifford, J. Cioslowski, B. B. Stefanov, G. Liu, A. Liashenko, P. Piskorz, I. Komaromi, R. L. Martin, D. J. Fox, T. Keith, M. A. Al-Laham, C. Y. Peng, A. Nanayakkara, M. Challacombe, P. M. W. Gill, B. Johnson, W. Chen, M. W. Wong, C. Gonzalez, and J. A. Pople, Computer Code GAUSSIAN 03, rev. C.01 (Gaussian, Inc., Wallingford CT, 2004).

[12] M. D. Wodrich, C. Corminboeuf, and P. v. R. Schleyer, Org. Lett. **8**, 3631 (2006).

[13] W. Kohn and L. J. Sham, Phys. Rev. **140**, A1133 (1965); S. H. Vosko, L. Wilk, and M. Nusair, Can. J. Phys. **58**, 1200 (1980).

[14] A. D. Becke, Phys. Rev. A **38**, 3098 (1988); C. Lee, W. Yang, and R. G. Parr, Phys. Rev. B **37**, 785 (1988); B. Miehlich, A. Savin, H. Stoll, and H. Preuss, Chem. Phys. Lett. **157**, 200 (1989).

[15] W. Nowacki and K. W. Hedberg, J. Am. Chem. Soc. **70**, 1497 (1948); I. Hargittai and K. W. Hedberg, J. Chem. Soc., Chem. Commun. **1972**, 1499; J. P. Amoureux, M. Bee, and J. C. Damien, Acta Crystallogr., Sect. B: Struct. Crystallogr. Cryst. Chem. **36**, 2633 (1980); J. P. Amoureux and M. Foulon, Acta Crystallogr., Sect. B: Struct. Sci. **43**, 470 (1987).

[16] M. Shen, H. F. Schaefer, C. Liang, J. Li, N. L. Allinger, and P. von R Schleyer, J. Am. Chem. Soc. **114**, 497 (1992).

[17] A. J. Lu, B. C. Pan, and J. G. Han, Phys. Rev. B **72**, 035447 (2005).

[18] G. C. McIntosh, M. Yoon, S. Berber, and D. Tomanek, Phys. Rev. B **70**, 045401 (2004).

[19] J. P. Perdew, K. Burke, and M. Ernzerhof, Phys. Rev. Lett. **77**, 3865 (1996); Phys. Rev. Lett. **78**, 1396(E) (1997).

[20] We do not consider the relaxation of adamantane for two reason. First, computationally it is still very challenging to simulate a substrate with over 100 atoms at a high theoretical level such as ours. Our main purpose is to first obtain an accurate potential surface for adamantane. Without such an accurate surface, it is not possible to investigate these relaxation effects. Second, adamantane is a hard material. Thus, the relaxation is expected to be very small [M. A. Lantz, H. J. Hug, R. Hoffmann, P. J. A. van Schendel, P. Kappenberger, S. Martin, A. Baratoff, and H.-J. Gntherodt, Science **291**, 2580 (2001)].

[21] F. J. Giessibl, Phys. Rev. B **56**, 16010 (1997); F. J. Giessibl and H. Bielefeldt, *ibid.* **61**, 9968 (2000); S. Morita, R. Wiesendanger, and E. Meyer, *Noncontact Atomic Force Microscopy* (Springer, Berlin, 2002); S. A. Burke, J. M. Mativetsky, R. Hoffmann, and P. Grutter, Phys. Rev. Lett. **94**, 096102 (2005); T. Kunstmann, A. Schlarb, M. Fendrich, Th. Wagner, R. Moller, and R. Hoffmann, Phys. Rev. B **71**, 121403(R) (2005); T. Fukuma, K. Kobayashi, K. Matsushige, and H. Yamada, Appl. Phys. Lett. **86**, 193108 (2005); **87**, 34101 (2005); B. W. Hoogenboom, P. L. T. M. Frederix, J. L. Yang, S. Martin, Y. Pellmont, M. Steinacher, S. Zäch, E. Langenbach, H.-J. Heimbeck, A. Engel, and H. J. Hug, *ibid.* **86**, 74101 (2005).

[22] D. Figgen, G. Rauhut, M. Dolg, and H. Stoll, Chem. Phys. **311**, 227 (2005).

[23] K. A. Peterson and C. Puzzarini, Theor. Chem. Acc. **114**, 283 (2005).

[24] S. Kotochigova, Z. H. Levine, E. L. Shirley, M. D. Stiles, and C. W. Clark, Phys. Rev. A **55**, 191 (1997); http://physics.nist.gov/PhysRefData/DFTdata/contents.html

[25] H.-J. Werner, P. J. Knowles, R. Lindh, F. R. Manby, M. Schütz, P. Celani, T. Korona, G. Rauhut, R. D. Amos, A. Bernhardsson, A. Berning, D. L. Cooper, M. J. O. Deegan, A. J. Dobbyn, F. Eckert, C. Hampel, G. Hetzer, A. W. Lloyd, S. J. McNicholas, W. Meyer, M. E. Mura, A. Nicklass, P. Palmieri, R. Pitzer, U. Schumann, H. Stoll, A. J. Stone, R. Tarroni, and T. Thorsteinsson, MOLPRO version 2006.1 (2006).